Stable structures of He and H_2O at high pressure

Hanyu Liu,[1] Yansun Yao,[1,2,*] and Dennis D. Klug[3]
[1]*Department of Physics and Engineering Physics, University of Saskatchewan, Saskatoon, Saskatchewan, Canada S7N 5E2*
[2]*Canadian Light Source, Saskatoon, Saskatchewan, Canada S7N 2V3*
[3]*National Research Council of Canada, Ottawa, Canada K1A 0R6*
(Received 4 September 2014; revised manuscript received 12 November 2014; published 7 January 2015)

The knowledge of the structures that can exist in compounds containing helium is of interest for understanding the conditions where and if this inert element can form structures where closed shell electrons of helium can participate in bonding that is not describable exclusively by van der Waals interactions alone. In this study we examine stable mixtures of He and H_2O at high pressures using a first-principles structure searching method. We find a thermodynamically stable structure that can be characterized by interactions comparable in strength to that of conventional hydrogen bonds. An orthorhombic structure with space group *Ibam* is identified that has progressively lower enthalpy with increasing pressure above 296 GPa than a mixture of He and H_2O. This mechanically and dynamically stable structure is found at pressures that are now becoming accessible to high-pressure techniques.

DOI: 10.1103/PhysRevB.91.014102 PACS number(s): 71.15.Mb, 62.50.−p, 81.05.Zx, 82.20.Wt

There is a very active discussion in the literature of the structures and properties of compounds formed with elemental systems, including the inert gases, at high pressures. These studies have uncovered and characterized, for example, numerous van der Waals (vdW) or chemically bound crystalline compounds for the heavier inert gases Ne, Ar, and Xe at high pressures. Where vdW interactions are dominating, these include mixed He-inert gas compounds such as $Ne(He)_2$ and $Ar(He)_2$ that were examined to pressures of about 20 GPa and N-He compounds [1–3]. As well, chemically bound, gas-phase metastable He compounds structures have been predicted [4]. More recently, possible stable compounds of xenon and iron have been searched for and predicted structures were found that may explain the missing Xe paradox in the earth [5]. In addition, Xe compounds such as XeF_2 can yield metallic character at high pressures [6]. He, on the other hand, has not yet been demonstrated to form thermodynamically stable compounds where there is actual negative formation enthalpy characteristic of compound structural stability. There are reports of filled ice structures [7,8] that can be also classified as stabilized via vdW and repulsive forces. These include the earlier report of a helium hydrate that closely resembles a high pressure form of ice, ice II [7]. In this material the He modifies the lattice parameters of ice II and could possibly be described as a filled ice II or helium hydrate structure. More recently, precise data on the solubility of He in the low pressure form of ice has been reported [8] and found that the solubility was much less than that for total occupation of voids in ice Ih which would imply one He atom per two water molecules. Structural data was not presented to verify if He filled ice could be analogous to the He filled ice II hydrate structure investigated by Londono *et al.* [7] although significant expansion of the ice Ih lattice occurs similar to that found for the He-ice II hydrate. It has recently been found in high-pressure experiments, and supported by *ab initio* calculations, that Xe forms a weakly metallic compound with H_2O ice above 50 GPa [9]. In the present study we therefore examine and characterize possible structures that He can form with H_2O, and in particular, to explore the degree to which the closed shell electrons of He can contribute to yield stable structures with bonding greater in strength than vdW interactions that dominate at low or moderately high pressures.

The search for crystalline structures of H_2O-He phases was performed using particle swarm optimization methodology as implemented in the CALYPSO program [10,11]. Recent successful applications of this method include examples of structure predictions for various crystalline systems (Ref. [12] and references therein). Structural optimizations, enthalpies, and electronic structures were calculated using the Vienna *ab initio* simulation (VASP) program [13] and projector-augmented plane wave (PAW) potentials employing the Perdew-Burke-Ernzerhof (PBE) functional [14]. The H, He, and O potentials have $1s^1$, $1s^2$, and $2s^22p^4$ as valence states, respectively, adopting an energy cutoff of 800 eV. Dense k-point meshes were employed to sample the first Brillouin zone (BZ) and ensured that energies converged to within 1 meV/atom. Phonon calculations were performed using the PHONOPY code [15]. A topological analysis of the electron density $\rho(\boldsymbol{r})$ has been carried out using the quantum theory of atoms-in-molecules (AIM) [16]. In the AIM theory, an atom within a solid is defined through the "zero-flux" condition of the electron density gradient $\nabla\rho(\boldsymbol{r})$. The analysis of the electron density and its curvatures at a bond critical point (BCP), i.e., the saddle point along a bond path, provides information about the type and properties of bonding. The AIM theory has been proven to be a useful tool in the characterization of interactions in closed-shell systems, such as ionic, hydrogen bonded, or vdW compounds [17].

Thermodynamic stabilities of various $(H_2O)_xHe_y$ phases have been investigated through their relative enthalpies of formation ΔH^f with respect to solid mixtures of H_2O and He. The ΔH^f has been calculated for every stoichiometry at 300 and 500 GPa, using the lowest-enthalpy structure obtained from the structure searches [Fig. 1(a)]. Here a negative ΔH^f indicates that the compound is more thermodynamically stable than the mixture, while the convex hull of ΔH^f connects all

*Author to whom correspondence should be addressed: yansun.yao@usask.ca

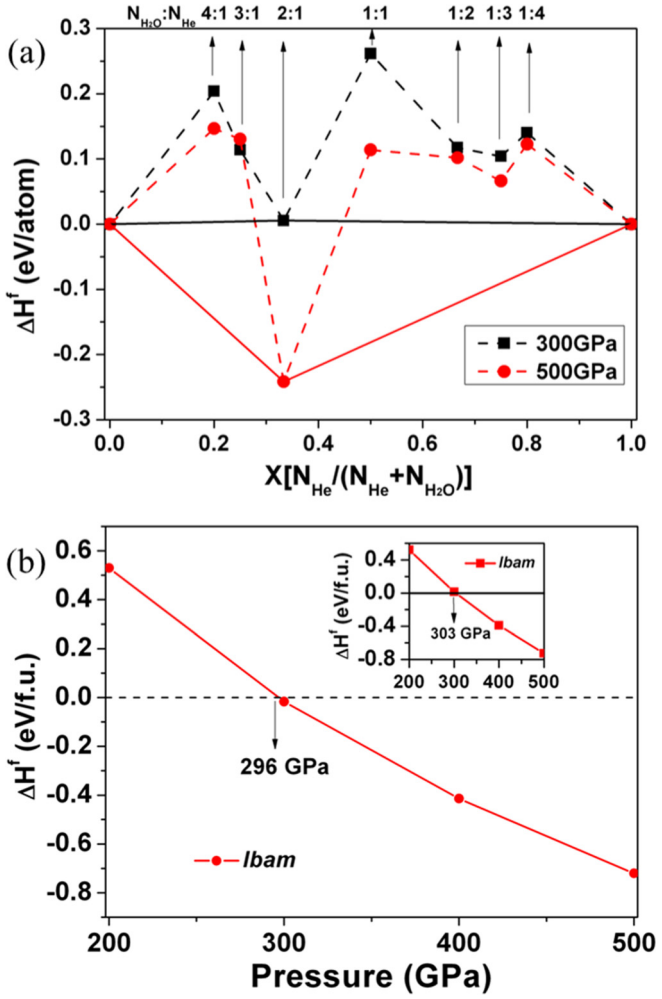

FIG. 1. (Color online) (a) Enthalpies of formation (ΔH^f, with respect to *Pbcm* H_2O and hexagonal close packed He) of the most stable $(H_2O)_xHe_y$ phases. A fractional representation $(H_2O)_{(1-x)}He_x$ $(0 < x < 1)$ is used such that $\Delta H^f[(H_2O)_{(1-x)}He_x] = H[(H_2O)_{(1-x)}He_x] - (1-x)H[H_2O] - xH[He]$. (b) The zero-point-energy corrected ΔH^f of the $(H_2O)_2He$ phase with respect to H_2O and He. Inset shows the ΔH^f without the zero-point-energy corrections (see text).

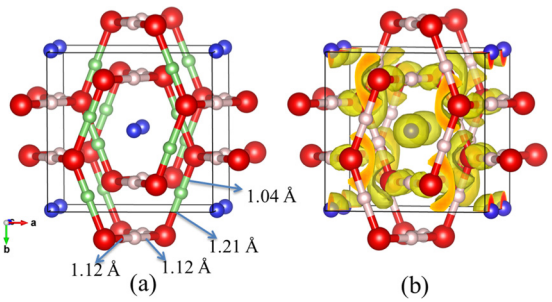

FIG. 2. (Color online) (a) *Ibam* crystal structure and (b) the same structure with the electron localization function (isovalue = 0.8) of $(H_2O)_2He$ at 300 GPa. Structures are viewed in a conventional unit cell. Green, pink, red, and blue spheres indicate H(1), H(2), O, and He atoms.

stable phases. The *Pbcm* structure of H_2O ice and hexagonal close packed structure of He [18] were used as reference structures. The *Pbcm* ice is the structure predicted to form at about 3 Mbars from ice X [19,20]. The energy difference between the *Pbcm* and ice X structure stable just below 3 Mbars is small and does not materially affect the convex hull calculations. In Fig. 1(a) the only identified stable stoichiometry for $(H_2O)_xHe_y$ compounds is $(H_2O)_2He$. The predicted $(H_2O)_2He$ phase has an orthorhombic structure (space group: *Ibam*), whose ΔH^f approaches zero near 300 GPa (∼0.005 eV/atom). At 500 GPa, its ΔH^f reaches ∼−0.24 eV/atom which confirms the stability of this phase under high pressure. Meanwhile, in the same pressure range, the ΔH^f of other $(H_2O)_xHe_y$ stoichiometries remain positive. The ΔH^f of the *Ibam* structure as a function of pressure is presented in the inset of Fig. 1(b), which shows that this phase becomes thermodynamically stable near 303 GPa. To account for the vdW interactions, the ΔH^f was recalculated using both semiempirical DFT-D2 vdW corrections [21] and the optB88-vdW density functional [22,23]. The results indicate that the vdW interactions only have minor effects on the energetics of the $(H_2O)_2He$ in the pressure range of interest. This is in contrast to the previously studied He filled ice and He-inert gas compounds where vdW interactions are significant. An inclusion of the vdW interactions slightly lowers the starting point of the stability of the *Ibam* structure, from 303 GPa (PBE) to 297 GPa (optB88-vdW), and to 291 GPa (DFT-D2) (see Appendix A). Due to the light atomic masses in $(H_2O)_2He$, the zero-point energy (ZPE) may be able to affect the phase stability. The ZPE was estimated for $(H_2O)_2He$, H_2O, and He using the harmonic approximation. Inclusion of the ZPE in the PBE calculations further stabilizes the *Ibam* structure with respect to H_2O and He reducing the starting point of its stability slightly to 296 GPa [Fig. 1(b)].

The *Ibam* structure is shown in Fig. 2(a). The structure parameters optimized at 300 GPa are: H(1)8*j* 0.242, 0.098, 0.0, H(2) 8*g* 0.0, 0.327, 0.25, *O* 8*j* 0.157, 0.329,0.0, and He 4*a* 0.5, 0.5, 0.25, with $a = 4.36$, $b = 4.19$, and $c = 3.51$ Å. A particularly interesting feature of this structure is the unsymmetric O–H–O bond lengths. In addition, the *Ibam* structure is distinctly different from that of ice VIII and ice X that is identified for pure H_2O ice at lower pressures. These structures are characterized as each consisting of two interpenetrating hydrogen-bonded networks related to the low-pressure cubic ice form, ice Ic. Ice VIII has hydrogen bonds characterized in a similar manner as that found in ice Ic, where the hydrogen atom in the hydrogen bond between neighboring oxygen atoms is located at about 1 Å from one oxygen atom and at a greater distance from the other oxygen atom. In ice X, the oxygen atoms in a hydrogen bond are at much shorter hydrogen-bonded distances than in ice VIII, resulting in a symmetric hydrogen bond with the proton in the center of the potential well between neighboring hydrogen bonded oxygen atoms. All O–H–O hydrogen-bond lengths are equal in ice X. The *Ibam* structure is distinctly different from the ice structures that form with hydrogen at lower pressures [24] where hydrogen molecules are suggested to replace one of the interpenetrating ice lattices in ice VIII.

In the *Ibam* structure the two interpenetrating lattices remain intact but He atoms are located in channels down the z axis of this structure [Fig. 2(a)]. The effect is to distort the hydrogen bond lengths in the x-y planes very slightly but also yielding distinctly different O–H bond lengths at 300 GPa of 1.036 and 1.208 Å. The total length of 2.244 Å for the O–H–O bond at 300 GPa in the *Ibam* structure corresponds to the calculated bond length at about 140 GPa for ice X [25]. *Ab initio* path integral calculations that followed the transformation of ice VII and VIII to ice X showed that protons become delocalized in the lower transition pressure range between that of ice VIII and ice X. For the O–H–O bond lengths at 300 GPa in the *Ibam* structure, however, the protons are expected to be localized in a single-well potential for pure ice based on the work of Benoit *et al.* [25] and a harmonic approximation would be appropriate. The distinctly different O–H lengths within hydrogen bonds in the *Ibam* structure reflects the role of He in its bonding; each He atom is surrounded by four H(1) atoms and two H(2) atoms, where the distances of He–H(1) and He–H(2) also differ and are found to be 1.435 and 1.368 Å. If the He atoms are removed from the *Ibam* structure, the structure is immediately unstable and transforms directly to the ice X structure during the geometry optimization. At even higher pressures of 400 and 500 GPa, the bond length difference in the O-H-O bonds in the $x-y$ plane persists with He present in the lattice indicating the role of the bonding property of He in the *Ibam* structure. The O-H-O distances are well within the distance range for ice X formation at these pressures so quantum tunneling effects would be expected to be present and modify slightly the pressure dependence of this structural detail. The He-H(1) and He-H(2) distances also remain slightly different even at 500 GPa. This behavior of $(H_2O)_2He$ is in direct contrast to the case of He filled ice II where removal of the He results only in a change of the modified Ice II lattice parameters directly to ice II host lattice parameters, and demonstrates the important role that He plays in stabilizing the $(H_2O)_2He$ compound.

The topological properties of the electron density $\rho(\boldsymbol{r})$ can provide an indication of whether the *Ibam* structure is fundamentally different than the vdW compounds that have been reported at lower pressures. At 300 GPa, each He atom is at distances of 1.773 and 1.875 Å from its nearest neighbor O atom. These distances are much shorter than the sum of the two vdW radii (2.92 Å). The quantum AIM analysis [26] identifies BCPs in the interatomic regions between He and O, suggesting a subtle but non-negligible bonding interaction. The calculated $\rho(\boldsymbol{r})$ at the BCPs are 0.45 and 0.35 e^-Å^{-3}, respectively, for the two nearest neighbor He···O paths. The values of $\rho(\boldsymbol{r})$ increase progressively with the pressure, as a consequence of bond shortening, to 0.73 and 0.70 e^-Å^{-3} at 1 TPa. To put this in perspective, the $\rho(\boldsymbol{r})$ for conventional hydrogen bonds fall in a range of 0.04 to 0.24 e^-Å^{-3}, at ambient pressure [17]. It therefore indicates that the strength of He···O interactions in the *Ibam* structure may be comparable to or potentially stronger than conventional hydrogen bonds. For the filled ice II hydrate, on the other hand, the calculated $\rho(\boldsymbol{r})$ along the nearest neighbor He···O paths are much smaller, i.e., about 0.02 e^-Å^{-3} at 4 kbars, which can be characterized as vdW interactions. The Laplacian $\nabla^2\rho(\boldsymbol{r})$ at the two BCPs are 9.22 and 6.53 e^-Å^{-5}, respectively, which clearly defines closed-shell interactions between He and its nearest neighbor O atoms. It is important for the $\nabla^2\rho(\boldsymbol{r})$ to be positive for the He···O interactions since these interactions are dominated by contraction of electrons away from the interatomic region toward each of the nuclei. The electron localization function [27] of the *Ibam* structure in Fig. 2(b) demonstrates this behavior; the tendency of electron localization between H_2O and He is very low. A positive $\nabla^2\rho(\boldsymbol{r})$ is a characteristic of closed-shell interactions [28]. It has been shown that the $\nabla^2\rho(\boldsymbol{r})$ of conventional hydrogen bonds falls in a range of 0.58 to 3.35 e^-Å^{-5} [17]. Thus, the He···O interaction in the *Ibam* structure appears to be stronger than the conventional hydrogen bonding, which is consistent with the analysis of $\rho(\boldsymbol{r})$. For the filled ice II hydrate, the calculated value of $\nabla^2\rho(\boldsymbol{r})$ are 0.40 and 0.32 e^-Å^{-5} (4 kbars), between the He and O atoms, clearly falling in the range for vdW interactions. From these topological properties, we therefore suggest a clear distinction between the He···O interaction in the *Ibam* structure and that of the filled ice II. The former is characterized as a strong, closed-shell, bonding interaction with the character and strength similar to that of

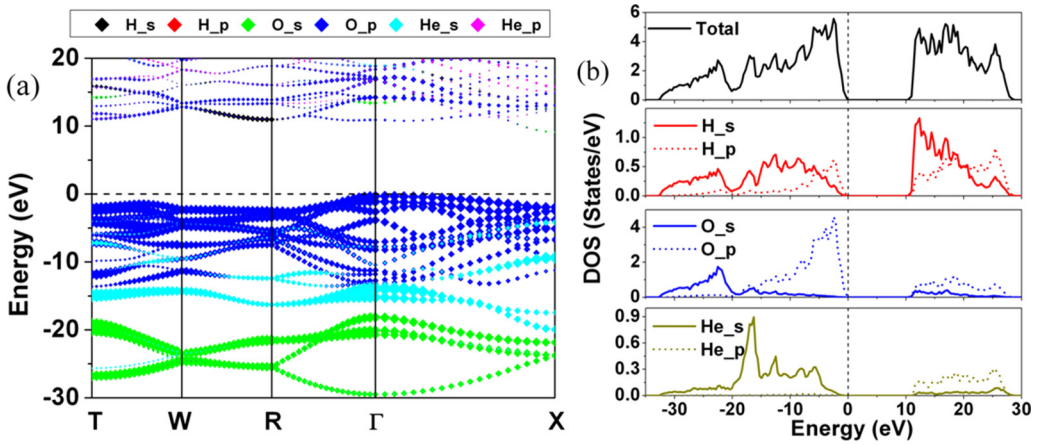

FIG. 3. (Color online) (a) Electronic band structure and (b) projected density of states for the *Ibam* structure of $(H_2O)_2He$ at 300 GPa. In (a), band characters from different orbitals are highlighted by a fat-band representation.

hydrogen bonds, while the latter is a vdW interaction. There is also a clear distinction between this He···O interaction and that of the covalent O-H bonds in a water molecule, and that of typical ionic bonds. We have analyzed the energetics for the BCPs in the *Ibam* structure, and compared it with the filled ice II vdW compound (Appendix B).

Ice is a wide band gap insulator at ambient conditions and at high pressures up to the TPa region. Because of the closed-shell nature of the He···O interactions, the presence of He in the ice does not lead to an immediate closure of the band gap. We have calculated the electronic band structure and projected density of states for the *Ibam* structure at 300 GPa [Figs. 3(a) and 3(b)], which reveal an indirect band gap of ∼10 eV between the Γ and *X* points. Similar to the ice, the electronic states of $(H_2O)_2He$ near the band gap are dominated by oxygen. The fat-band representation [Fig. 3(a)] clearly shows three subsets of valence bands, which, in the order of decreasing energy, are characteristic of O 2*p* orbital (0 to −20 eV), He 1*s* orbital (−5 to −20 eV), and O 2*s* orbital (−20 to −30 eV). The bands of hydrogen mix strongly with those of oxygen throughout the valence regime, representing an O–H–O covalent network. The bands of He consist primarily of its 1*s* orbitals, which mix with the bands of oxygen, in particular, between −5 and −15 eV, for a bonding He···O interaction. These properties suggest weak interaction between H_2O and He and that an interaction similar in strength to hydrogen bonding is playing a significant role in stabilizing the $(H_2O)_2He$ at high pressures. In addition, the stability of the *Ibam* structure at high pressures has been established from the phonon calculations (Fig. 4). The absence of imaginary frequencies confirms that this structure is dynamically stable and therefore experimentally accessible.

It is worth noting that another recent theoretical and experimental work reports an interesting result that Na_2He can be formed at high pressures [29]. However, the origin of $(H_2O)_2He$ structural stability is distinctly different from that of Na_2He under high pressure. For the reported cubic phase Na_2He, transferred electrons from metallic Na atoms to He atoms play the key role in stabilizing its structure, where this mechanism is similar to the pure Na system in its hp4 high-pressure insulating structure [30] where the origin of stability is due to a valence electron transferred into interstitial space forming an electride. In the Na_2He electride, paired electrons are located in interstices in the structure taking on the role of anions and also yield an insulating structure. In contrast, in the

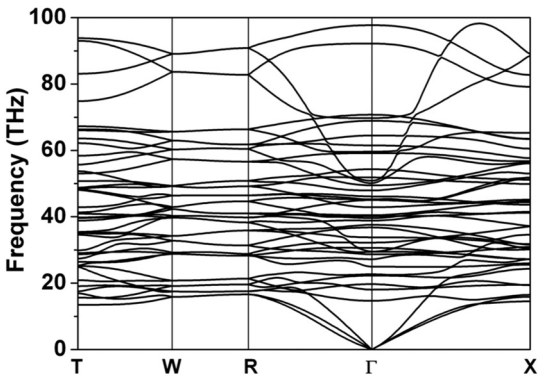

FIG. 4. Phonon band structure for the *Ibam* structure of $(H_2O)_2He$ at 300 GPa and 0 K.

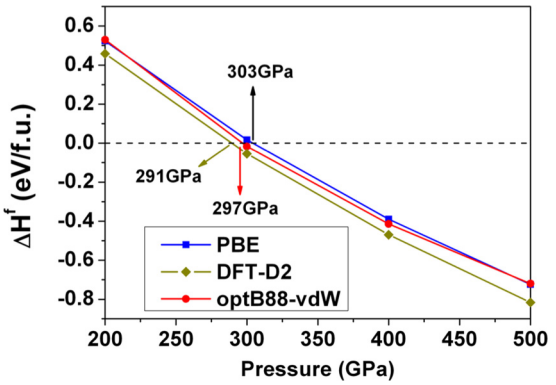

FIG. 5. (Color online) Enthalpies of formation (ΔH^f, with respect to H_2O and He) of the $(H_2O)_2He$ phase (*Ibam* structure), calculated using the optB88-vdW, DFT-D2, and PBE schemes.

$(H_2O)_2He$ compound, there is little electronic charge transfer between H_2O and He atoms but direct He···O interactions of closed-shell nature play the critical role of stabilizing the *Ibam* structure under high pressure. As an approximate measure, the calculated Bader charges (at 300 GPa) for H(1), H(2), O, and He atoms in the *Ibam* structure are 0.3619, 0.3782, 9.2465, and 2.0286 e^-, respectively, which only suggests a minor amount, i.e., ∼0.0286 e^-, of charge transfer from H_2O to He. The critical role of He is seen where its removal from the *Ibam* structure at 300 GPa results in a direct transformation to the ice X structure with symmetric hydrogen bonds.

In summary, we have investigated the conditions at which the closed-shell electrons of helium exhibits near neighbor interactions in a dynamically stable $(H_2O)_2He$ high-pressure structure. We have found, by employing a particle swarm search method, an orthorhombic *Ibam* insulating $(H_2O)_2He$ structure that exhibits unique structural properties including a mixture of symmetric and nonsymmetric hydrogen bonds. This structure is distinctly different from the He filled ice or hydrates defined by vdW interactions alone in that He is essential for the *Ibam* structure. It is shown that helium at 300 GPa exhibits bonding properties with H_2O that are not characterized as

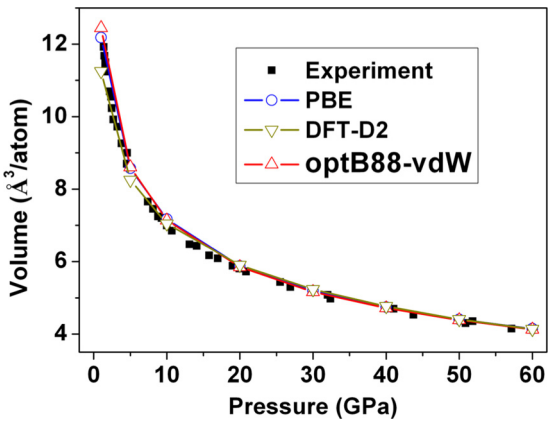

FIG. 6. (Color online) Theoretical (present results) and experimental equations of states for solid helium. The theoretical pressure-volume curves were obtained using the optB88-vdW, DFT-D2, and PBE schemes.

TABLE I. Topological properties of the BCP at the shortest He···O contacts (strong closed-shell interactions) and the shortest H-O contacts (covalent bonds) for the *Ibam* structure at 300 GPa. Multiplicity indicates the number of the He···O contacts connected to a single He atom.

Bond type	d(Å)	Multiplicity	$\rho(r_{BCP})$ (e^-Å^{-3})	$\nabla^2\rho(r_{BCP})$ (e^-Å^{-5})	G (kJ mol^{-1})	V (kJ mol^{-1})	E_{BD} (kJ mol^{-1})
He···O	1.773	3	0.4448	9.2156	248.41	−245.82	122.91
	1.875	3	0.3473	6.5303	172.25	−166.64	83.32
H-O	1.037		2.0451	−53.7068	55.53	−1573.85	786.93
	1.116		1.6266	−24.3684	261.27	−1186.27	591.14
	1.207		1.2414	−5.9734	340.08	−842.86	421.43

vdW interactions but have a strength and properties similar to that of hydrogen bonds in dense ice phases. We also note that the process of fusion that occurs in stars such as our Sun produces enormous quantities of helium resulting from the fusion reaction. Helium is the second most abundant element followed by oxygen in the Milky Way galaxy for example. It is therefore expected that there may be many exoplanetary bodies that contain large amounts of He and water and the structure we predict should be a significant component.

This project was supported by Natural Sciences and Engineering Research Council of Canada (NSERC) through a Discovery Grant.

APPENDIX A: EFFECTS OF THE VAN DER WAALS INTERACTIONS

Density functional theory is a well-established method for the characterization of atomic interactions in matters. In principle, density functional theory can yield exact ground-state energy of any correlated electronic system. In practice, however, approximations must be made for how electrons interact with each other in the system. These interactions are approximated by the exchange-correlation functionals. The local density approximation (LDA), generalized gradient approximation (GGA), and the hybrid functionals are among the most successful approximations developed over the years; the PBE functional [14] used in the present study is a realization of the GGA. The standard exchange-correlation functionals are known to lack the description for long-range dispersion interactions, colloquially referred to as the van der Waals (vdW) interactions, which originate from the instantaneous fluctuations of the electron distributions. The vdW interactions can contribute significantly to the phase stability of rare-gas solids, molecular crystals, and many other systems. These interactions may also have some effects on the $(H_2O)_2He$ compound.

We calculated the enthalpies of formation for the $(H_2O)_2He$ compound using (1) a van der Waals density functional (vdW-DF), optB88-vdW [22,23], (2) a semiempirical approach for vdW corrections, DFT-D2 [21], to account for the dispersion interactions, and (3) the standard PBE functional without any vdW corrections. The results are compared in Fig. 5 which shows that the vdW interactions only have minor effects on the energetics of the $(H_2O)_2He$ compound. An inclusion of the vdW interactions slightly lowers the pressure where the $(H_2O)_2He$ compound becomes stable, from 303 GPa (PBE) to 297 GPa (optB88-vdW), and to 291 GPa (DFT-D2). To this end, the standard PBE functional appears to be a reliable choice for the characterization of the $(H_2O)_2He$ compound in the pressure range of interest. Moreover, we also calculated the equation of the states of solid helium, using the optB88-vdW, DFT-D2, and PBE schemes, and compared the results with the available experimental data [31] in Fig. 6. All three schemes yield results that are in good agreement with the experiments. At low pressures the DFT-D2 is shown to outperform the optB88-vdW and PBE, whereas at the pressures above 20 GPa the three schemes yield essentially identical results which correspond remarkably well with the experiments, indicating a decrease of dispersion interactions with increasing pressure. This finding is consistent with the previous density functional calculations [32] which show that the PBE functional can provide the equation of state of helium in excellent agreement with the experiments.

APPENDIX B: TOPOLOGICAL ANALYSIS OF THE ELECTRON DENSITY

Topological analysis of all-electron charge density was carried out using the quantum theory of atoms-in-molecules. In

TABLE II. Topological properties of the BCP at the shortest He···O contacts (van der Waals interactions) and the OH···O contacts (hydrogen bonds) for the helium filled ice II structure at 4 kbars. Multiplicity indicates the number of the He···O contacts connected to a single He atom.

Bond type	d(Å)	Multiplicity	$\rho(r_{BCP})$ (e^-Å^{-3})	$\nabla^2\rho(r_{BCP})$ (e^-Å^{-5})	G (kJ mol^{-1})	V (kJ mol^{-1})	E_{BD} (kJ mol^{-1})
He···O	2.982	3	0.0243	0.4041	7.98	−4.94	2.47
	3.077	3	0.0199	0.3157	6.19	−3.78	1.89
OH···O	1.713		0.3188	3.0559	102.03	−120.82	60.41
	1.747		0.2904	3.0431	95.09	−107.31	53.66
	1.794		0.2561	2.6913	81.17	−89.05	44.53

TABLE III. Evolution of the topological properties of the BCP at the shortest He···O contacts for the *Ibam* structure under pressure. Multiplicity indicates the number of the He···O contacts connected to a single He atom.

Bond type	Pressure	d(Å)	Multiplicity	$\rho(r_{\mathrm{BCP}})$ (e^-Å^{-3})	$\nabla^2\rho(r_{\mathrm{BCP}})$ (e^-Å^{-5})	G (kJ mol^{-1})	V (kJ mol^{-1})	H (kJ mol^{-1})
He···O	300 GPa	1.773	3	0.4448	9.2156	248.41	−245.82	2.59
		1.875	3	0.3473	6.5303	172.25	−166.64	5.61
He···O	500 GPa	1.694	3	0.5438	11.5461	322.98	−331.49	−8.51
		1.756	3	0.4675	9.2076	255.28	−259.77	−4.49
He···O	1000 GPa	1.588	3	0.7265	16.6745	486.44	−518.71	−32.37
		1.598	3	0.7018	16.6779	476.21	−498.16	−21.95

this theory quantum mechanics is extended to open systems in which an atom within a solid is defined by a zero-flux surface of the electron density gradient $\nabla\rho(\boldsymbol{r})$. The charge density distribution $\rho(\boldsymbol{r})$ and its principal curvatures (three eigenvalues of the Hessian matrix) at the bond critical point (BCP), i.e., the saddle point between two atoms, reveal information about the type and properties of bonding. For the last two decades, the quantum theory of atoms-in-molecules has been successfully applied for the characterization of bonding in a variety of solid state systems [17]. Closed-shell interatomic interactions can be adequately described and classified by the topological properties of the electron density $\rho(\boldsymbol{r})$ at the (3, −1) BCP, where the density gradient $\nabla\rho(\boldsymbol{r})$ vanishes. The second derivative of the electron density (Laplacian) $\nabla^2\rho(\boldsymbol{r})$ reveals information about the concentration or depletion of the elections at the BCP. It has been shown that the $\nabla\rho(\boldsymbol{r})$ and $\nabla^2\rho(\boldsymbol{r})$ at the BCP are directly related to the bond order and thus to the bond strength [33], for which the bond dissociation energy (E_{BD}) can be estimated using the potential energy density V (r_{BCP}), i.e., $E_{\mathrm{BD}} = -\frac{1}{2}V(r_{\mathrm{BCP}})$. Here we used the virial theorem which relates the V (r_{BCP}) and the kinetic energy density G (r_{BCP}) to the $\nabla^2\rho(r_{\mathrm{BCP}})$, such as,

$$V(r_{\mathrm{BCP}}) = \frac{\hbar^2}{4m}\nabla^2\rho(r_{\mathrm{BCP}}) - 2G(r_{\mathrm{BCP}}) \tag{B1}$$

For a closed-shell interaction, G (r_{BCP}) can be obtained directly from $\nabla^2\rho(r_{\mathrm{BCP}})$ and $\rho(r_{\mathrm{BCP}})$,

$$G(r_{\mathrm{BCP}}) = \tfrac{3}{10}(3\pi^2)^{2/3}\rho^{5/3}(r_{\mathrm{BCP}}) + \tfrac{1}{6}\nabla^2\rho(r_{\mathrm{BCP}}) \tag{B2}$$

Since V (r_{BCP}) is always negative and G (r_{BCP}) always positive, the sign of the local energy density H (r_{BCP}) = G (r_{BCP}) + V (r_{BCP}) reveals which energy term dominates an interaction. Closed-shell interactions such as those previously found in ionic, hydrogen bonded or van der Waals systems have positive values of H (r_{BCP}), where shared electron density causes destabilization rather than stabilization of the system. Calculated topological properties of the electron density for the interatomic interactions in $(H_2O)_2He$ and He filled ice II are in Tables I –III.

[1] C. Cazorla, D. Errandonea, and E. Sola, Phys. Rev. B **80**, 064105 (2009).
[2] P. Loubeyre, M. Jean-Louis, R. LeToullec, and L. Charon-Gérard, Phys. Rev. Lett. **70**, 178 (1993).
[3] W. L. Vos, L. W. Finger, R. J. Hemley, J. Z. Hu, H. K. Mao, and J. A. Schouten, Nature (London) **358**, 46 (1992).
[4] Z. Bihary, G. M. Chaban, and R. B. Gerber, J. Chem. Phys. **117**, 5105 (2002).
[5] L. Zhu, H. Liu, C. J. Pickard, G. Zou, and Y. Ma, Nat. Chem. **6**, 644 (2014).
[6] M. Kim, M. Debessai, and C.- S. Yoo, Nat. Chem. **2**, 784 (2010).
[7] D. Londono, J. L. Finney, and W. F. Kuhs, J. Chem. Phys. **97**, 547 (1992).
[8] A. V. Ildyakov, A. Yu. Manakov, E. Ya. Aladko, V. I. Kosyakov, and V. A. Shestakov, J. Phys. Chem. B **117**, 7756 (2013).
[9] C. Sanloup, S. A. Bonev, M. Hochlaf, and H. E. Maynard-Casely, Phys. Rev. Lett. **110**, 265501 (2013).
[10] Y. Wang, J. Lv, L. Zhu, and Y. Ma, Phys. Rev. B **82**, 094116 (2010).
[11] Y. Wang, J. Lv, L. Zhu, and Y. Ma, Comput. Phys. Commun. **183**, 2063 (2012).
[12] Y. Wang and Y. Ma, J. Chem. Phys. **140**, 040901 (2014).
[13] G. Kresse and J. Furthmüller, Phys. Rev. B **54**, 11169 (1996).
[14] J. P. Perdew, K. Burke, and M. Ernzerhof, Phys. Rev. Lett. **77**, 3865 (1996).
[15] A. Togo, F. Oba, and I. Tanaka, Phys. Rev. B **78**, 134106 (2008).
[16] R. F. W. Bader, *Atoms in Molecules—A Quantum Theory* (Oxford University Press, Oxford, 1990).
[17] U. Koch and P. L. A. Popelier, J. Phys. Chem. **99**, 9747 (1995).
[18] J. M. McMahon, M. A. Morales, C. Pierleoni, and D. M. Ceperley, Rev. Mod. Phys. **84**, 1607 (2012).
[19] M. Benoit, M. Bernasconi, P. Focher, and M. Parrinello, Phys. Rev. Lett. **76**, 2934 (1996).
[20] B. Militzer and H. F. Wilson, Phys. Rev. Lett. **105**, 195701 (2010).
[21] S. Grimme, J. Comput. Chem. **27**, 1787 (2006).
[22] J. Klimeš, D. R. Bowler, and A. Michaelides, J. Phys.: Condens. Matter **22**, 022201 (2010).
[23] J. Klimeš, D. R. Bowler, and A. Michaelides, Phys. Rev. B **83**, 195131 (2011).
[24] W. L. Vos, L. W. Finger, R. J. Hemley, and H-K. Mao, Phys. Rev. Lett. **71**, 3150 (1993).
[25] M. Benoit, D. Marx, and M. Parrinello, Nature (London) **392**, 258 (1998).

[26] A. Otero-de-la-Roza, M. A. Blanco, A. Martín Pendás, and V. Luaña, Comput. Phys. Commun. **180**, 157 (2009).
[27] A. D. Becke and K. E. Edgecombe, J. Chem Phys. **92**, 5397 (1990).
[28] D. Cremer and E. Kraka, Angew. Chem., Int. Ed. Engl. **23**, 627 (1984).
[29] X. Dong, A. R. Oganov, A. F. Goncharov, E. Stavrou, S. Lobanov, G. Saleh, G.-R. Qian, Q. Zhu, C. Gatti, X.-F. Zhou, V. Prakapenka, Z. Konôpková, and H.-T. Wang, arXiv:1309.3827.
[30] Y. Ma, M. Eremets, A. R. Oganov, Y. Xie, I. Trojan, S. Medvedev, A. O. Lyakhov, M. Valle, and V Prakapenka, Nature (London) **458**, 182 (2009).
[31] C.-S. Zha, H.-K. Mao, and R. J. Hemley, Phys. Rev. B **70**, 174107 (2004).
[32] Z. Nabi, L. Vitos, B. Johansson, and R. Ahuja, Phys. Rev. B **72**, 172102 (2005).
[33] K. B. Wiberg, R. F. W. Bader, and C. D. H. Lau, J. Am. Chem. Soc. **109**, 1001 (1987).